Forecasting Research

Short-Range Forecasting Research
Scientific Note No. 20

MESOSCALE MODEL EXPERIMENTAL FORECASTS OF THE HAAR OF NORTH EAST SCOTLAND

by
S.P. Ballard, B.W. Golding and R.N.B. Smith

August 1990

ORGS UKMO S Duplicate
National Meteorological Library
FitzRoy Road, Exeter, Devon. EX1 3PB

Meteorological Office (Met O 11)
London Road, Bracknell, Berkshire RG12 2SZ, England

Met O 11 Scientific Note No 20

Mesoscale Model Experimental Forecasts of the Haar of North East Scotland

by

S P Ballard, B W Golding and R N B Smith

METEOROLOGICAL OFFICE.

Short Range Forecasting Research Division, Sci. Note No.20
Mesoscale model experimental forecasts of the Haar of north east Scotland.

AUGUST 1990

00061290 551.509.325

Short Range Forecasting Research Division
Meteorological Office
London Road
Bracknell
Berkshire
United Kingdom

NB This paper has not been published. Permission to quote from it must be obtained from the above Meteorological Office Division.

Mesoscale Model Experimental Forecasts of the Haar of North East Scotland

S P Ballard, B W Golding and R N B Smith

Meteorological Office, Bracknell, U.K.

August 1990

NOTE: This paper describes forecasts using the August 1988 version of the mesoscale model , objective analysis and interpolation of the regional (fine-mesh 1985 or 1986 version) model.

ABSTRACT

A mesoscale model is used to simulate the diurnal evolution of sea fog off the N.E. Scottish coast observed on 27 April 1984. It is shown that the accuracy of the early part of the forecast is very dependent on the specification of the initial conditions. If the initial description of the fog is sufficiently good the model can accurately erode it during the day and reform it in the following evening. The dependence of the accuracy of the forecasts on vertical resolution is also discussed.

1. Introduction

Forecasting of the formation, evolution and dispersal of fog is one of the most difficult problems facing local forecasters in many parts of the world. The United Kingdom Meteorological Office (UKMO) mesoscale model, (Golding 1987a, 1987b, 1990), with its very fine resolution and carrying of cloud water as a prognostic variable, is the first operational, three dimensional numerical forecasting model potentially able to address this problem directly. This paper assesses the ability of the model to capture the observed characteristics and evolution of sea fog, locally known as Haar, in the Moray Firth area of N.E. Scotland on 27 April 1984 (fig. 1). The case considered was one of three studied in a field project reported by Findlater, Roach and McHugh (1989), referred to as FRH in the rest of the text, which provides a detailed description of the properties of the fog. The diurnal evolution is simulated by running 18 hour forecasts from 0600 UTC 27 April 1984. This paper describes the formulation of the model, the observed structure and evolution of the fog, the sensitivity of the forecast to the initial conditions, comparisons between the forecast and the observations and its sensitivity to vertical resolution.

2. Model Formulation

The UKMO mesoscale model uses the non-hydrostatic adiabatic formulation of Tapp and White (1976) with the terrain following coordinate scheme of Carpenter (1979) and a suite of parameterizations of diabatic processes (Golding 1987b). Here, discussion will be limited to those processes that have been identified as being important for the prediction of fog (Brown and Roach, 1976, Musson-Genon, (1987), Tremant (1989), Cotton and Anthes (1990).

In order to incorporate cloud water in a consistent manner in the advection and turbulent mixing code, the model uses conserved thermodynamic variables, namely the liquid water potential temperature, θ_L ($\theta_L \equiv \theta - L\, q_L/c_p\pi$ where θ is the potential temperature, L is the latent heat of evaporation, π the Exner pressure function and q_L is the cloud water mixing ratio) and the total water, q_t ($q_t \equiv q + q_L$ where q is the humidity mixing ratio).

The turbulent mixing parametrization is based on the $1\frac{1}{2}$ order closure of Yamada and Mellor (1979) (their level 2.5 model), modified to include the effects of sub-grid scale saturation. The closure is obtained by neglecting all material time derivatives in the equations for second order correlations of turbulent quantities except for the turbulent kinetic energy, E ($E = \frac{1}{2}(\bar{u}'^2 + \bar{v}'^2 + \bar{w}'^2)$ where primes denote turbulent deviations from the mean). The fluxes are given by

$$\overline{w'\theta'_L} = -K_h \frac{\partial \theta_L}{\partial z}$$

$$\overline{w'q'_t} = -K_h \frac{\partial q_t}{\partial z}$$

$$\overline{w'\underline{v}'_H} = -K_m \frac{\partial \underline{v}_H}{\partial z}$$

where $\underline{v}_H = (u, v)$ is the horizontal velocity vector and the turbulent transport coefficients are given in terms of E and length scales by

$$K_h = l_h\, E^{\frac{1}{2}} \;,\; l_h = l_h\,(l,\, E,\, N^2,\, S^2)$$

$$K_m = l_m E^{\frac{1}{2}} , l_m = l_m (l, E, N^2, S^2)$$

l_m and l_h are given in Appendix A. The buoyancy N^2 is given by

$$N^2 = \bar{\beta}_T \frac{\partial \theta_L}{\partial z} + \bar{\beta}_w \frac{\partial q_t}{\partial z}$$

where $\bar{\beta}_T = \beta_T - \bar{a}_L \bar{b}_L c_f \beta_L$, $\bar{\beta}_w = \beta_w + \bar{a}_L c_f \beta_L$ and

$$\beta_T = \frac{g}{\theta} , \beta_w = \frac{0.608g}{1 + 0.608q - q_L} , \beta_L = \frac{L}{c_p \pi} \beta_T - \frac{\beta_w}{0.378}$$

c_f is the cloud fraction

$$\bar{a}_L = \frac{1}{1 + L\alpha_L / c_p} , \bar{b}_L = \alpha_L \pi$$

$$\alpha_L = \frac{\partial q_s}{\partial T} |_{T=T_L} = \frac{(0.622 L q_s (T_L) P)}{(R T_L^2 (P - 0.378 e_s(T_L))}$$

S^2 is the shear $| \partial \underline{v}_H / \partial z |^2$. The length scale, l, is given by the Blackadar formula

$$\frac{1}{l} = \frac{1}{kz} + \frac{1}{\lambda}$$

where k is Von Karman's constant. λ is specified for elevated as well as boundary layer turbulence by setting it equal to one third of the depth of the turbulent layer containing the height z. In the model the lower limit for this depth is the model layer thickness.

The turbulent kinetic energy E is given by the prognostic equation

$$\frac{DE}{Dt} = -\overline{w' \underline{v}'_H} \cdot \frac{\partial \underline{v}_H}{\partial z} + \frac{g}{\theta_v} \overline{w' \theta'_v} - \frac{1}{\varrho} \frac{\partial}{\partial z} (\varrho \overline{w' E}) - \frac{E}{\tau_o}$$

where $\theta_v = \theta(1 + 0.608q - q_L)$ is the virtual potential temperature, and τ_o is a dissipation timescale. The first of these terms represents shear effects, the second represents buoyancy effects, the third represents turbulent transport and the last is the dissipation.

The dissipation timescale τ_o is given by

$$\tau_o = \frac{c_o l}{\sqrt{E + F_L l^2 N^2}}$$

where c_o and F_L are empirically determined dimensionless constants. The stability dependent term $F_L l^2 N^2$ is included to give the same asymptotic stability dependence as André et al (1987) and Sun and Ogura (1980).

The turbulent kinetic energy flux is obtained by forming its prognostic equation and simplifying following Therry and Lacarrère (1983) to give

$$\overline{w'E} = \tau_4 \left[-\overline{w'^2} \frac{\partial E}{\partial z} + \frac{1}{2} \frac{g}{\theta_v} \overline{w'^2 \theta'_v} \right]$$

Here, the first term represents down-gradient transport and the second term represents buoyancy effects. The latter is parametrised using simplified forms of prognostic equations for the third order correlations involving w' and θ'_v to give

$$\overline{w'E} = -K_E \frac{\partial E}{\partial z} - K_B \left[\bar{\beta}_T \frac{\partial}{\partial z} \left(\overline{w'\theta'_L} \right) + \bar{\beta}_w \frac{\partial}{\partial z} \left(\overline{w'q'_t} \right) \right] - K_C \left[\bar{\beta}_T^2 \frac{\overline{\partial \theta'^2_L}}{\partial z} + 2\bar{\beta}_T \bar{\beta}_w \frac{\overline{\partial \theta'_L q'_t}}{\partial_z} + \overline{\beta_w^2} \frac{\overline{\partial q'^2_t}}{\partial z} \right]$$

where K_E, K_B K_C and the variances and covariances of θ_L and q_t are given in Appendix B.

The remaining unknown in the scheme is a means of diagnosing θ, q, q_L from θ_L, q_t. This is performed following Sommeria and Deardorff (1977). Using expressions for the variances of θ_L, q_t, and an approximation to the saturated value of q derived from θ_L, formulae are derived for the mean and variance of the sub grid scale distribution of supersaturation S.

$$\bar{S} = \bar{a}_L \left(q_t - q_{sL}(T_L) \right)$$

$$\sigma_s^2 = \bar{a}_L^2 \left(\overline{q'^2_t} - 2\, \bar{b}_L \overline{q'_t \theta'_L} + \bar{b}_L^2 \overline{\theta'^2_L} \right)$$

A "top hat" probability distribution with mean $\bar{S}$ and variance σ_s^2 is then used to diagnose the fraction of the grid volume that is saturated, and hence the liquid water, humidity and potential temperature. The results are generally insensitive to the distribution used. Smith (1990), in adapting the scheme for the UKMO atmospheric general circulation model, used a triangular probability distribution function. The two distributions are compared in Smith (1984). The "top hat" form is particularly economical to use, though it is theoretically less satisfactory than the normal distribution used by Sommeria and Deardorff (1977)).

In order to ensure smooth evolution of the fluxes, a backward implicit time integration scheme is used for this part of the model.

The precipitation parametrization has been described in Golding (1987a, 1987b and 1990). Rain is formed from water cloud by two processes, local production and accretion of rain falling through the layer. The former process is based on the scheme of Sundqvist (1978). Evaporation of rainfall is calculated using a formula based on Rutledge and Hobbs (1983). Of significance here, is the inclusion of droplet settling at the lowest model level. A linear approximation to the fall velocity is made which is approximately valid for the range of liquid water mixing ratios commonly encountered:

$$V = 0.01 + 90\, m_c$$

where m_c is the average liquid water mixing ratio in the cloudy fraction of the grid volume.

Radiative processes are important to all stages of fog development (Pilie et al 1979, Cotton and Anthes 1990). For a mature fog such as that studied here, the radiative budget at fog top is of particular importance. The model parametrization computes radiation budgets at the land surface and at the (highest) cloud top. The short wave transmission to the ground is computed by applying, multiplicatively, empirical transmission functions for Rayleigh scattering, water vapour absorption, aerosol scattering and cloud. Each is expressed as an exponential so as to produce an efficient code. For cloud, the transmission is a function of $\sqrt{w}$, where w is the integrated liquid water mixing ratio, fitted to computations using the model of Slingo and Shrecker (1982). In broken cloud, clear and cloudy transmissions are combined, the latter being weighted by the square of the maximum cloud fraction. An albedo of 0.18 was used in the experiments reported here. The long wave budget at the ground consists of a downward cloud component which is a function of total liquid water path and the cloud base temperature; a downward clear sky component computed from the total water vapour path and the mean temperature below 500m; and black body emission at the surface temperature. At cloud top, the downward long wave flux

is computed from the total liquid water path and the cloud top temperature (T_{cT}). The upward long wave fluxe uses the same temperature but is dependent on the liquid water path ($q_L \Delta z$) in the highest cloud layer only. Thus the long wave budget may be written (after Lind and Katsaros 1982) as

$$L = \sigma \{[1 - exp(-70 q_L \Delta z)] - [0.157 \, log \, \hat{Q} + 0.611]\} \, T_{cT}^4$$

where $\hat{Q}$ is the optical path length in $kg \, m^{-2}$.

Since the absorption depth of short wave radiation in cloud can be large, it is not appropriate to compute the absorption in the highest layer only. A simplified form is therefore used:

$$S = S_o \, cos \, z \, (0.07 + 0.15 \, cos \, z)$$

where S_o is the solar flux at the top of the atmosphere and z is the solar zenith angle. On the basis that the dominant effect of the solar absorption is to reduce the net long wave cooling during daylight, S is constrained to not exceed L.

The ground surface temperature is predicted from the surface energy budget over land but is held constant throughout the forecast over sea.

The formulation of the surface fluxes follows that described by Carpenter (1979). Drag coefficients for heat and momentum are computed as a function of roughness length and Richardson number using Monin–Obukhov formulae. The roughness length for momentum was prescribed as 10cm over land for these experiments and was computed using the windspeed dependent formula of Charnock (1955) over the sea. The roughness length for heat and moisture was set at one fifth of that for momentum. Consistent with the use of conservative variables in the turbulent diffusion scheme, the surface fluxes are defined in terms of θ_L and q_t, and the Richardson number is written as:

$$R_i = g z_1 [(\theta_{L1} - \theta_*)/\theta_1 + (q_{t1} - q_*)/(q_1 + \alpha)]/ \mid \underline{u}_1 \mid^2, \; \alpha = 0.608$$

where θ_* is the surface potential temperature and q_* is the surface humidity defined implicitly using a surface resistance to evaporation following Monteith (1964). Over the sea the surface air is assumed saturated but over land, the resistance was set to $100s\ m^{-1}$ by day and $500s\ m^{-1}$ at night.

For presentation, the surface temperature (at 1.25m) was diagnosed using a stability dependent interpolation between the ground/sea surface and the first model level (Golding 1990). Visibility was diagnosed from the liquid water content and relative humidity using an estimate of the low level aerosol concentration predicted by the model (Golding 1990).

The experiments reported here were performed with a 50×50 grid having a horizontal resolution of 15 km on a transverse Mercator projection centred on longitude 2°W. The orography of the central part of the model domain is shown in figure 1 with crosses marking the grid points. In this paper, the name Moray Firth is used to refer to the whole sea area west of a line from Wick to Peterhead. The initial experiments were made with a 16 level configuration of the model; later comparisons used a 29 level configuration (figure 2). Boundary conditions were obtained from temporal and spatial interpolations of forecast fields from the UKMO operational regional model (75 km grid spacing).

3. Synoptic Situation

During an anticyclonic period in late April 1984, (figure 3), sea fog developed in the Atlantic west of Ireland. This was advected round the north of Scotland into the North Sea and Moray Firth. It spread southwards to reach the Netherlands and to affect the whole east coast of the U.K. Late on 27 April the anticyclone had moved over the North Sea causing the fog to retreat northwards again influenced by the S.S.E. winds. A heat low formed during the morning and afternoon of 27 April over the Scottish mainland producing local modification of the wind field.

4. Observations of the Haar on 27 April 1984

Observations of the structure and evolution of the fog on 27 April 1984 were

provided by the conventional synoptic surface observations and radiosondes as well as by satellite imagery, and by data obtained from a minisonde at Lossiemouth and from the Meteorological Research Flight Hercules aircraft (as described by FRH).

The full extent of the sea fog on 27 April can be seen in the 0836 UTC NOAA-8 visible satellite image in figure 4a. It extended from the Atlantic Ocean, north of Scotland, to the North Sea and into the Moray Firth. Radiative cooling from the fog top had by this time cooled the fog below the sea temperature so that it was convectively well mixed. The convective nature of the fog top was evident in enlargements of the satellite imagery. During the night of the 26/27 April the fog had spread onto the low lying land of the eastern coastal plain and further inland into the valleys of the North-west Highlands and the Grampians (figure 4a). The surface observations (figure 5) showed the presence of fog at all observing stations in eastern Scotland at 0600 UTC. The 0000 UTC 27 April Shanwell and Lerwick radiosonde ascents and Lossiemouth minisonde data showed that the fog was about 300 m deep near the coasts overnight.

During the morning rapid heating of the land caused the fog to clear from all but a narrow coastal strip where it was maintained by a light south easterly wind. The fog also cleared from southern parts of the Moray Firth as can be seen in the 1448 UTC satellite image in figure 4b. Aircraft observations showed that the fog cleared the southern coast of the Moray Firth from the east. The fog depth at Lossiemouth decreased from 0800 UTC onwards clearing completely by 1615 UTC. Where the fog persisted near the coast temperatures remained below 10°C. Inland temperatures reached 25°C by the afternoon and a heat low developed with an associated wind circulation, (figure 5b). Aircraft measurements of the fog top height taken during the afternoon, (figure 6), showed that it increased from the coast towards the centre of the Moray Firth where it was 250–275 m. There was a steep gradient across the mouth of the Moray Firth and the top was higher than 375 m in the North Sea. Also, as can be seen from figure 6, the fog top continued dropping during the afternoon over the whole area.

The fog reformed on the coastal plain and inland valleys during the evening and following night as can be seen in figure 5c. The fog had returned to Lossiemouth by 1830 UTC. Midnight coastal ascents again showed fog depths of about 300 m. The satellite image on the morning of 28 April was similar to figure 4a.

Vertical profiles taken through the fog near mid-day showed a steep inversion of 10–12 deg C at fog top and near-saturated adiabatic lapse rates in the fog. Profiles of liquid water content were close to that expected from adiabatic ascent, extrapolation to the surface indicated that the base was mainly 20–60 m above the sea surface but in some instances did reach the surface. Turbulence was experienced throughout the fog but above it, wind profiles became smoother and characteristic of a stable atmosphere. Profiles taken in regions of deep and shallow fog are shown in figure 7. The locations are shown in figure 1.

FRH concluded that after a period of development during transport over a relatively cold sea, an initially 'warm' advection fog tends to become a diurnally modulated, self-maintaining 'cold' radiation fog held at a temperature 1–2 deg C below sea surface temperature. The radiative cooling depresses the temperature of the fog far enough below sea surface temperature that the cooling becomes balanced by latent and sensible convective heat input from the sea surface. The movement and moulding of the fog is influenced by diurnally forced wind systems such as the circulation associated with a heat low.

They suggested that the well-defined clearance of the Haar in the southern part of the Moray Firth in the afternoon appeared to be due to an off-shore wind developing there in association with the circulation around the heat depression over the Scottish mainland.

5. Sensitivity of forecast to initial conditions

Accurate initial conditions are vital if a good forecast is to be obtained, especially in the case of sea fog or low cloud. In anticyclonic conditions they can often be regarded as passive systems moved and moulded by local winds. The dependence of low cloud forecasts on good initial conditions was investigated by Wright and Golding (1990). In this section,

the sensitivity of forecasts of fog to initial conditions is studied.

In the routine operation of the UKMO mesoscale model, initial conditions are provided by using surface, radar and satellite observations to modify mesoscale background fields. These are obtained by combining fields from the latest UKMO regional model forecast with three hour forecasts of cloud, boundary layer structure and other small scale detail from the mesoscale model (Wright and Golding 1990, Golding 1990). For this case study no prior mesoscale forecast was available; the background fields were therefore obtained by interpolating onto the mesoscale grid, the 6 hour regional model forecast from 0000 UTC 27 April 1984 (figure 8a). The regional model does not predict cloud water explicitly so this was inferred where the relative humidity exceeded 95% (98% below 20m). The amount of cloud water inserted was related to the forecast precipitation rate and cloud depth. As can be seen from figure 8a the fields obtained were generally in good agreement with observations except for the humidity distribution. Although fog was correctly indicated in the Moray Firth and the Central Lowlands, the analysis indicated surface air that was too dry over the North Sea and too moist to the west and north of Scotland. In the Moray Firth the analysed fog extended from the surface to 110m. Over the North Sea analysed bases were at 310m and tops at 610m. There was little fog or low cloud analysed south of Peterhead.

Not surprisingly, perhaps, the mesoscale forecast from these initial conditions had a poor representation of the evolution of the sea fog (figure 8). All fog was lost from inland areas, the Moray Firth and the North Sea early in the forecast. By 1500 UTC there was only some shallow fog forecast to remain to the north west of Scotland and small patches of low cloud forecast between the Orkneys and Shetlands and over the North Sea due east of the Firth of Forth. However by midnight the forecast low cloud had been advected further north, spread over a wider area and the bases had lowered to the surface. The patch in the North Sea, with top at 110m, had been forecast to advect north westward so that it lay to the east of Peterhead by midnight. Also by this time fog was forecast in the

east of Scotland and North East England along windward, southeast or east facing coasts, spreading inland where model elevations were below 300m. Despite the poor forecast of the evolution of the sea fog, reasonable agreement was obtained with the surface observations over land during the night apart from the more sheltered north facing coast of the Moray Firth and near Shanwell and the Firth of Forth where the forecast erroneously remained fog free.

Better initial conditions were produced (figure 9a) using objective analyses of the surface synoptic observations. The analysis method is described in Golding (1984). Analyses of the screen level humidity, visibility and cloud cover, type and base were used to modify the humidity, cloud cover and cloud water fields on the basis of conceptual models. Fog depth was diagnosed by the following method. Where "sky obscured" was reported, the fog top height was set to 210 m, or to the top of any low cloud in the background field if higher. Otherwise the fog top height was set to 60m and all cloud removed or set to be consistent with the cloud reports. The lack of observations over the sea and the mountains resulted in a poor analysis of the extent of the fog. However fog was correctly added along the East coasts of Scotland and N. England and removed from the west and north.

The forecast from these improved conditions, (figure 9), was slightly better than that from the interpolated regional model fields. The forecast fog persisted longer over land clearing most inland areas by 1200 UTC and the Moray Firth by 0900 UTC. The small area of fog over the North Sea soon lifted to give low cloud. However more low cloud was retained over the North Sea to the north east of the Moray Firth than in figure 8. This may be due to a better initialisation of cloud water. The later parts of the forecast were similar to the original but with larger areas of fog forecast over the North Sea and around Shanwell and the Firth of Forth and some low cloud in the Moray Firth.

In order to further improve the initial conditions, manual intervention was performed on the cloud water, cloud fraction and relative humidity fields. This used information from the 0836 UTC satellite image, the radiosonde and minisonde ascents and the Meteorological

Research Flight aircraft data, in addition to the surface observations, to define the areal extent, depth and vertical structure of the fog.

The 0836 UTC satellite image was used to define the edge of the fog over the North Sea and to the north of Scotland. Since the satellite image was valid for two and a half hours later than the data time of the forecast it was assumed that the fog would have extended further up the valleys at the earlier time. The east facing 300 m contour of the mesoscale orography provided a good match with the estimated inland fog edge.

Although the aircraft observations showed a gradient in fog top height between the coast, the Moray Firth and the North Sea during the day, it was assumed that the fog depth had been more uniform during the night. This is consistent with FRH's finding that the sharp gradient in fog depth off Peterhead was less steep during the morning than the afternoon and with the theory that the heat low circulation was responsible for the localised clearance of the fog; with no localised subsistence during the night the fog depth should be more uniform.

The observations of fog depth suggested a nighttime value of between 300 and 375 m over the sea. The fog top height was taken to be 340 m above sea level everywhere.

Inside the fog area the cloud fraction was set to 8 octas at all model levels up to the fog top. The liquid water profile was assumed to be adiabatic from the ground to fog top consistent with the aircraft observations in FRH. The adiabatic profile was approximated as a gradient of 2g $kg^{-1}km^{-1}$ starting from zero at the ground and reaching values of about 0.6g kg^{-1} at the fog top over the sea. The relative humidity was set to 100% at all points inside the fog.

Outside the fog area, and above the fog top, the cloud fraction and cloud liquid water were set to zero and the relative humidity was limited to a maximum value of 95%. These modified initial conditions are shown in figure 10a. The forecast from the modified initial conditions retained most of the inserted moisture showing that they were adequately

close to balance with the new humidity field. The model retained the sea fog throughout the forecast period and during the day the fog only lifted off the surface around its edges and to the south east of the Orkneys. The fog cleared from the land during the morning and, in the Moray Firth, it cleared northwards from the south coast. The fog returned overland during the evening. The fog cleared from the south coast of the Moray Firth rather too early and too extensively and retreated too far northwards over the North Sea though in general the forecast evolution of the fog was good. The distribution of the fog at 1500 UTC and 0000 UTC is shown in figures 10b) and 10c). This provided much better guidance during the day than the previous forecasts as it indicated that sea fog was going to affect windward facing coasts. The forecast was sufficiently accurate to allow the study of the diurnal evolution of the fog and a detailed comparison with the observations. That is described in the following section.

6. More detailed comparison of mesoscale model forecast with observations

With an accurate forecast of the clearance of the fog from inland areas during the day the model gave a good indication of the observed temperature distribution as can be seen by comparison of figures 10b and 5b. At 1500 UTC the model had forecast temperatures up to 22°C inland and below 10°C on the coast where the fog has been retained or lifted to low stratus. No values as high as the 24.7°C observed in the Grampians were forecast; this is probably the result of the inability of the model to represent the valley sites of the observing stations. Temperatures were predicted to be 6–7°C over the sea which verify well with some of the coastal observations. However, temperatures predicted on the coast near Lossiemouth were too high due to the erroneous clearance of the fog in that area.

The model produced a good forecast of the formation of the inland heat low (figure 11). A double centred low was predicted, centred over the North-west Highlands and Grampians, which compared well with the subjective analysis of the surface observations shown in FRH. Comparison of figures 10a, b shows the development of the associated wind circulation modifying the predominantly south easterly synoptic flow.

By midnight the surface winds were forecast to be returning to south easterly as the heat low circulation diminishes. Again at this time, due to the good prediction of the inland penetration of the fog at night, the forecast temperatures were in general agreement with the observations as can be seen by comparison of figures 10c and 5c. Temperatures were forecast to be above 10°C in the fog free western side of Scotland and less than 5°C in the east in fog inland from the windward facing coasts.

The diurnal evolution of the fog was generally predicted quite well. The fog was correctly predicted to clear from the land during the day and to persist over the North Sea. Reformation of the fog inland was predicted on windward sides of the mountains during the evening, the distribution verifying well with the available surface observations and with the 0814 UTC 28 April satellite image. Comparing figures 1 and 10c it appears that the predicted inland fog edge roughly followed the 300 m orographic height contour. However, the southern edge over the North Sea was predicted to retreat too far north compared with the 0814 UTC satellite image and during the day the model predicted too much clearance of fog in the Moray Firth. This also occurred too early and proceeded from west to east rather than east to west as was observed. Nevertheless mist (visibility 1–5 km) was predicted throughout much of the Moray Firth at 1500 UTC, see figure 12, and the area of visibility greater than 10 km agreed well with the observed clearance in the 1448 UTC satellite image. FRH suggested that the subsidence was enhanced in the observed clear area due to the modification of the synoptic wind field by the circulation associated with the inland heat low. They showed, from the aircraft observations, that

the region of most rapid retreat of the fog edge roughly corresponded with the region of highest inferred subsidence. In the model, the forecast vertical velocity at 210m had a local maximum in the area of highest visibilities, thus supporting FRH's conclusion. Forecast values of subsidence of 1.5–2.2 cms^{-1} in this area between 1200 UTC and 1500 UTC agree well with FRH's value of $2cms^{-1}$ based on the observed rate of fog top descent.

During the early afternoon the forecast topography of the fog top agreed well with the observations considering the limited vertical resolution of this version of the model. It showed a gradient in fog top height across the mouth of the Moray Firth, steeper in the south than in the north. The fog top was also predicted to decrease between 1200 UTC and 1500 UTC in roughly the same area as shown in the observations. The fog lifted off the surface around the edge to give a base of 110 m. This agrees fairly well with the observations of bases of mainly 20–60 m in the Moray Firth area. The evolution of the topography of the fog top is shown in figure 13.

By midnight, when the fog reformed in the Moray Firth, it had a depth of 110 m dropping to 10 m on the edge of the fog. The top remained at 310 m over the North Sea, and rose to this height in the mouth of the Moray Firth. The tops were predicted to be 310m at Shanwell and Lerwick which agreed well with the midnight radiosonde ascents. The base was predicted to fall to the surface throughout most of the observed fog area.

Figures 14a and b show profiles of temperature, dew point, cloud liquid water and turbulent kinetic energy from the model at 0600, 1200 UTC 27 April and 0000 UTC 28 April at the locations of α and β marked on figure 1. The profiles at 1200 UTC can be compared with figure 7. Within the fog the temperature profiles are predicted to be close to the saturated adiabatic lapse rate and the near surface temperatures are 1.75°C and 0.5°C below the model's sea surface temperature at α and β respectively. Although both locations were initialised with a 310 m fog top, by 1200 UTC the profile at β was only saturated to 110 m though at α there was still a clearly defined top at 310 m. Within the resolution of the model this is broadly in agreement with the observations of fog tops of about 350 m and

220 m respectively indicating that the model has captured the observed spatial variation in fog top. Although all positions were initialised with cloud liquid water increasing to 0.5g/kg at fog top this has decreased at both locations by 1200 UTC. Significant levels of turbulent kinetic energy were only forecast within the fog layer in agreement with the observations. The fog top temperatures at both locations also agreed quite well with the values of 3°C in the North Sea and 4.5–5°C in the Moray Firth reported in FRH. However it is evident that the vertical resolution of the model was not sufficient to define the fog top accurately. It does not allow a sharp enough inversion, although warming at 610 m has made it sharper than is the initial conditions, and the fog top lay between model levels at α and β. By midnight at both locations the model has further strengthened the inversion as the temperature rose at 610 m and dropped within the fog by 0.25 to 0.5°C. The model predicted further drying out above the inversion whilst the amount of cloud liquid water and turbulent kinetic energy rose, presumably because the drop in temperature allowed more convective mixing. At β the predicted fog was shallower and denser than at α where the fog was colder.

The correspondence between the predicted and observed wind profiles was not as good as for the temperature and humidity. The predicted winds at midday at α were south easterly up to 610 m and north-easterly above whereas observed winds were southerly at all levels up to 800 m. At β the winds were predicted to be south-easterly up to 1010 m whereas observed winds backed to north-easterly above 400 m. Stream line analyses from the aircraft observations at 150 m showed south-easterly winds over most of the sampling area, weakening and backing to become north-easterly to the west of Lossiemouth. The forecast wind field at 110 m agreed well with the observations, the flow being very similar to the surface winds. However above 400 m there was less agreement with the observations which showed a broad north-easterly flow that weakened towards Wick to become south-westerly. In the forecast at 610 m the winds were still south-easterly in the mouth of the Moray Firth and weakened and veered to become south-westerly to the west of Lossiemouth.

The forecast winds only had a northerly component inland south of the Moray Firth. At 850 mb the forecast wind was north-easterly over the Moray Firth region in agreement with the observations. The predicted winds fields above 400 m were similar to those from the operational regional model forecast that provided the synoptic forcing.

7. Sensitivity of forecast to higher vertical resolution

In order to try to obtain better definition of the vertical structure of the fog, the experimental forecast was rerun with a 29 level version of the model. The levels are shown in figure 2 in comparison with the 16 level version. They provide far better resolution in the near surface layers where the fog formed. The initial conditions were essentially the same as in the best 16 level forecast described above. The regional model fields were interpolated to the 29 levels over the same 15 km horizontal grid. The intervention was then performed in the same way using the same fog area and cloud water profile, the only difference being that the highest level with cloud was 340 m rather than 310 m due to the different spacing of the model levels.

The linear horizontal diffusion included in the model to remove the grid splitting of the centred advection scheme caused problems near the ground in steep orography because of the high vertical resolution. These were avoided by applying the diffusion along the terrain following model surfaces in the lowest four levels; successful smooth forecasts were then achieved.

Over the sea the forecast fog area was very similar to that from the 16 level version, fog being retained over the North Sea but still clearing from too large an area of the Moray Firth during the day. At 1500 UTC the forecast visibilities at 10 m in the inner part of the Moray Firth were slightly higher than in the 16 level version but were lower elsewhere in the area shown in figure 12. The region of clearance in the observations was marked by forecast visibilities above about 8 km and corresponded with the region of highest forecast subsidence. The fog base was forecast to rise above 10 m over a wider area during the

day. Nearly all the fog was forecast to lift off the surface by 1800 UTC but by midnight the forecast fog base had lowered to the surface and there was very little difference from the 16 level version. Forecast winds were also very similar apart from a reduction in the 10 m windspeed across the mouth of the Moray Firth. In areas forecast to be cloud free there was little difference in screen temperatures during the day but by midnight the 29 level version was better with values greater than 15°C predicted in some areas on the West Coast. However, too much fog was retained inland from the windward coasts during the day and too much formed over the Grampians at night. Also more precipitation was produced from the fog and the temperature dropped to 0°C at midnight in the fog to the east of the North-West Highlands. These deficiencies may indicate that the physical parameteriations needed to be improved to cope with the higher vertical resolution.

As expected the extra levels allowed better resolution of the fog over the sea, (figure 15). At 1200 UTC more low cloud/lifted fog was retained in the Moray Firth on the edge of the fog bank. The fog top height distribution, and its change between 1200 UTC and 1500 UTC was in better agreement with the observations. The predicted fog top fell below 300 m over a wider area but below 200m over a smaller area than in the 16 level version. By midnight as in the 16 level version, the forecast fog tops had risen again. A smaller area rose to above 300 m than in the 16 level version but throughout the Moray Firth the tops rose to 250 m with some higher tops near the coast. Again the forecast agreed well with the coastal radiosonde ascents.

As can be seen from comparison of figures 16 and 14 the profiles through the fog showed much better resolution of the fog top. The inversions were much sharper. At 1200 UTC, the cloud tops of 340 m and 250 m respectively at α and β are in much better agreement with the observed heights. However, the cloud water at α and β did not peak at these levels but at 250 and 175 m respectively, though by 1500 UTC the cloud tops had dropped to those heights. By midnight the fog tops rose again to 340 and 250 m. At β the cloud water content increased at all levels but at α it declined at all levels apart

from 340 m and the base lifted off the surface to 40 m. The base had also lifted at β to 70 m during the late afternoon and early evening, when the top dropped to 115 m, but it descended to the surface again by midnight. The lifted fog bases agreed fairly well with the observations of 20–60 m. Profiles taken at points in the model in the Moray Firth where the fog cleared totally showed that it reformed first at the inversion height and then the base dropped to the surface.

8. Discussion

The results of section 5 show the importance of obtaining a good initialisation of the cloud water and humidity fields if the evolution of the sea fog and its impact on visibilities and temperatures is to be forecast. The benefits that accrue from the use of satellite imagery and colocated profile data from radiosondes, minisondes or aircraft ascents to define the areal extent and vertical structure of the fog is clearly demonstrated.

These experiments provided one of the incentives for the development of a more elaborate mesoscale initialisation system (Wright and Golding, 1990 and Golding 1990) which includes the objective use of satellite data to define cloud tops and cloud cover. However, even if this system had been available for this experiment, it is clear that additional human intervention would have been needed due to difficulties in identifying fog in an objective system. A conceptual model, based on this case study, has been developed to allow the initialisation of a cold, well mixed fog from analyses of surface visibility, surface air temperature, fog top height and a definition of the areal extent of the fog. The model is then initialised with a saturated adiabatic lapse rate, from the surface air temperature, between the surface and the fog top height along with an adiabatic cloud water profile, total cloud cover and 100% relative humidity. Further development and testing of this scheme is planned for the future.

In the experiments described in sections 5 to 8 no attempt was made to modify the initial temperature structure in the model. The initial profiles did not have the sharp

inversion at fog top evident in all the measured profiles. One experiment was performed with the 29 level version of the model in which, as well as modifying the cloud water field the temperature and humidity profiles up to 1900 m within the fog area were modified on the basis of the 0830 UTC Lossiemouth minisonde data and midnight Shanwell radiosonde ascent. The same profile was set at all points in the fog area. The forecast for 1500 UTC retained more fog in the Moray Firth to the north and west of Lossiemouth than the original. However it could not be directly compared with the forecasts in section 5 as the dynamical balance in the model was upset because the modification of the temperature field was not accompanied by appropriate modifications to the thermal wind field. Spurious winds were predicted in the early part of the forecast so that at 0900 UTC at low levels they were westerly and northerly above 700 m. By 1500 UTC they were in better agreement with the observations than the original run as the winds had settled to south-easterly at levels near 150 m and were predominantly north-easterly near 750 m. This demonstrates the need for careful balancing of the fields when they are modified through intervention techniques.

Despite the absence of the sea fog during the day in the forecasts from data interpolated from regional model fields, the model forecast the fog forming inland from windward facing coasts during the evening. This appears to be due to the combined effect of moister air being advected from the southeast together with surface radiative cooling after sunset. Some sea fog was also forecast to return during the evening which further improved the verification of the later stages of these forecasts. Patches of fog in the initial conditions lifted to stratus during the day and were advected with the prevailing wind. After sunset the cloud cooled radiatively which allowed it to deepen towards the surface. During the day this process was suppressed by absorption of solar radiation.

Given a realistic specification of the initial cloud water and humidity fields a good forecast of the diurnal evolution of the Haar was obtained. The model representation of surface fluxes, turbulent mixing, radiative cooling and precipitation processes are suffi-

ciently realistic to allow the bulk of the fog to be maintained. The results support the opinion of FRH that the fog was maintained by radiative cooling from fog top, balanced by convective transport of latent and sensible heat input from the sea surface. In the model the fog was indeed colder than the sea surface temperature and turbulent throughout its depth. At night when radiative cooling was no longer balanced by solar heating the fog cooled further and the turbulent kinetic energy increased indicating more convective mixing. This also agrees with the conclusions of Pilie et al. 1979, from studies of deep marine fog along the California coast, that vertical turbulent mixing can contribute positively to the growth of fog when it occurs in the presence of radiative cooling.

A weakness of the forecast was that too little fog was maintained in the western part of the Moray Firth during the day. However, results in this area were sensitive to the initialisation of the temperature inversion and to the level and form of horizontal diffusion. In fact, forecasts in that area are a severe test of the initial conditions, the boundary layer parametrisations, the modelling of flow in complex terrain and the limited horizontal resolution of the model. Only a few model grid points cover the sea in that area and there are steep changes in orographic height inland. No sensitivity tests have been performed with the physical parametrisations and it is possible that improvements would allow the maintenance of fog in that area. The relevance of the errors in the prediction of wind direction to the forecast in that area is unclear since the errors occurred above fog top. However, it is possible that the observed onshore winds above fog top may have assisted its maintenance whereas the predicted offshore winds assisted its clearance. It is also possible that local variations in sea surface temperature may have been influential in that area in view of the role of sea surface temperature in the formation and maintenance of sea fog (Pilie et al 1979, FRH, Tremant 1989). The observed distribution on 1 May 1984 after the fog had cleared showed temperatures of about 7°C in the northern part of the Moray Firth area but increasing from a local minimum of 5°C off Peterhead to 9°C in the south western edge of the Moray Firth. The model distribution did not have this contrast. Values were

near 7°C everywhere but with a slight east-west temperature gradient of 6.9°C to 7.3°C along the southern edge of the Moray Firth. In the experiment described in section 6, the forecast air temperatures of 8 to 9°C at 1500 UTC were higher than the model's sea temperatures west of Lossiemouth but sea surface temperatures of 9°C may have been sufficient to allow the maintenance of fog.

9. Conclusion

The results of these simulations show that when the mesoscale model is initialised with good humidity and cloud water profiles and has accurate synoptic forcing it can forecast the diurnal evolution of sea fog.

During the early part of the forecast, (daytime), the accuracy was very dependent on the initial conditions. However in the later stages of the forecast, during the evening and night, the accuracy was less dependent on the initial conditions as longwave radiative cooling from the land surface and cloud top allowed fog to develop.

The precise details of the forecast in the inner Moray Firth were not well predicted but may be sensitive to the physical parametrisations, numerical formulation, resolution and sea surface temperature. Although insufficient fog was predicted in that area the heat low and surface wind field were well predicted and so could have been used by a forecaster with knowledge of the existing extent of sea fog in the area to predict the likely evolution.

The benefits of greater vertical resolution in the model were also demonstrated.

Acknowledgements

We should like to thank W.R.P. Taylor who ran some of the early simulations for this case study, J. Findlater, Dr. W.T. Roach, Dr. P. White and Dr. P. Ryder for encouraging us to develop the work for publication and Miss J. Blackburn for typing the text.

Appendix A

Length scales used in the turbulent transport coefficients

The length scales l_h and l_m in the diffusion coefficients K_h and K_m in section 2 are given by

$$l_h = \frac{\frac{2}{3} c_2 \, E^{\frac{1}{2}} \, (E + F_L \, l^2 \, N^2)^{\frac{1}{2}} \, l}{\left\{ E + F_3 \, l^2 \, N^2 + F_o \, l^2 \, S^2 \left[\frac{E + F_2 \, l^2 \, N^2}{E + F_1 \, l^2 \, N^2} \right] \right\}}$$

$$l_m = l_h \, \frac{c_1}{c_2} \, \frac{[E + F_2 \, l^2 \, N^2]}{[E + F_1 \, l^2 \, N^2]}$$

where $F_o = \frac{2}{3} c_1^2$, $F_1 = c_1 \, c_2 + F_L$

$$F_2 = (1 - a_2) \, c_2 \, (2 \, c_3 - c_2) + F_L$$

$$F_3 = 2 \, c_2 \left[(1 - a_2) \, c_3 + \frac{2}{3} c_1 \right] + F_L$$

c_i are empirically determined nondimensional constants relating all timescales so that $\tau_i = c_i \, \tau$ and $\tau_o = c_o \, \tau$ is given in section 2.

$c_o = 5.52427$, $c_1 = 1.04694$, $c_2 = 1.41337$, $c_3 = 3.08492$ and $F_L = 7.09759$.

From Launder (1975) $a_2 = \frac{1}{3}$.

Appendix B

Coefficients, variances and covariances used in the vertical flux of turbulent kinetic energy

The coefficients in the expression for the vertical flux of turbulent kinetic energy given in section 2 are given by

$$K_E = \frac{\tau_4[(1+\tau_8\,\tau_9\,N^2+4\tau_6\tau_8N^2)\overline{w'^2}\;+\;(1+\tau_8\tau_9N^2)\tau_6\;\overline{w'B'}}{[1+\tau_8\tau_9N^2)(1+\tau_4\tau_6N^2)\;+\;4\tau_6\tau_8N^2]}$$

$$K_B = \frac{\tau_4\tau_6[(1+\tau_8\tau_9N^2)\overline{w'^2}\;+\;\tau_8\;\overline{w'B'}]}{[(1+\tau_8\tau_9N^2)(1+\tau_4\tau_6N^2)+4\tau_6\tau_8N^2]}$$

$$K_C = \frac{\tau_4\tau_6\tau_8[\overline{w'^2}\;+\;\tau_9\;\overline{w'B'}]}{[(1+\tau_8\tau_9N^2)(1+\tau_4\tau_6N^2)+4\tau_6\tau_8N^2]}$$

where $\overline{w'B'} \equiv \frac{g}{\theta_v}\,\overline{w'\theta_v}' = -K_h\,N^2$.

$$\overline{w'^2} = \frac{2}{3}\,\bar{E} + \frac{2}{3}\,\tau_1\,[\,\overline{w'\underline{v}_H}\;\frac{\partial v_H}{\partial z} + 2\,\frac{g}{\theta_v}\,\overline{w'\theta_v}'\,]$$

Again the timesales are all taken to be proportional to the master timescale τ given in section 2. The constant c_4 is chosen so that, in neutral conditions $K_E = K_m$ i.e. $c_4 = c_1$.

The remaining constants are $c_6 = c_8 = 0.81c_4$ and $c_9 = 3c_8$.

The variances and covariances of θ_L and q_t required in the calculation of the vertical flux of turbulent kinetic energy are given by

$$\overline{\theta_L'^2} = -\,2\,\tau_3\,\overline{w'\theta_L'}\;\frac{\partial\theta_L}{\partial z}$$

$$\overline{q_t'^2} = -\,2\,\tau_3\,\overline{w'q_t'}\;\frac{\partial q_t}{\partial z}$$

$$\overline{\theta_L'q_t'} = -\tau_3\left[\overline{w'\theta_L}'\,\frac{\partial q_t}{\partial z} + \overline{w'q_t}'\,\frac{\partial\theta_L}{\partial z}\right]$$

where $\tau_3 = \frac{c_3}{c_o}\,\tau_o$, $c_3 = 3.08492$.

REFERENCES

André, J.C., de Moor, G., Lacarrère, P., Therry, G. and du Vachat, R., 1978: Modelling the 24-hour evolution of the mean and turbulent structures of the a.b.l. *J. Atmos. Sci.*, 35, 1861.

Brown, R. and Roach, W.T., 1976: The physics of radiation fog: II – A numerical study. *Quart. J. R. Meteor. Soc.*, 102, 335–354.

Carpenter, K.M., 1979: An experiment using a non-hydrostatic mesoscale model. *Quart. J. R. Meteor. Soc.*, 105, 629–655.

Charnock, H., 1955: Wind stress on a water surface. *Quart. J. R. Meteor. Soc.*, 81, 639–640.

Cotton, W.R. and Anthes, R.A., 1989: *Storm and cloud dynamics.* San Diego, Academic Press, 303-328.

Findlater, J., Roach, W.T. and McHugh, B.C., 1989: The Haar of north-east Scotland. *Quart. J. R. Meteor. Soc.*, 115, 581–608.

Golding, B.W., 1984: The Meteorological office mesoscale model, its current status, *Meteor. Mag.*, 113, 288–302.

Golding, B.W., 1987a: Short Range Forecasting over the United Kingdom using a Mesoscale Forecasting System, *Short - and Medium- range Numerical Weather Prediction*, ed. T. Matsuno, Meteor. Soc Japan, 563–572.

Golding, B.W., 1987b: The U.K. Meteorological Office Mesoscale Model, *Boundary Layer Meteor.*, 41, 97–107.

Golding, B.W., 1989: A simple two phase precipitation scheme for use in numerical weather prediction models. Met.O.11 Scientific Note No.13 (Unpublished, copy available in National Meteorological Library, Meteorological Office, Bracknell, Berkshire, RG12 2SZ, England).

Golding, B.W., 1990: The Meteorological Office mesoscale model. *Meteor. Mag.*, 119, 81–96.

Launder, B.E., 1975: On the effects of a gravitational field on the turbulent transport of heat and momentum. *J. Fluid Mech.*, 67, 569.

Lind, R.J. and Katsaros, K.B., 1982: A model of longwave radiance for use with surface observations. *J. Appl. Meteor.*, 21, 1015–1024.

Monteith, J.L., 1964: Evaporation and environment. *Symp. Soc. Exp. Bio.*, 19, 205–234.

Musson-Genon, L., 1987: Numerical simulation of a fog event with a one-dimensional boundary layer model. *Mon. Wea. Rev.*, 115, 592–607.

Pilie, R.J., Mack, E.J., Rogers, C.W., Katz, U. and Kocmond, W.C., 1979: The formation of marine fog and the development of fog-stratus along the California Coast. *J. Appl. Meteor.*, 18, 1275–1286.

Rutledge, S.A. and Hobbs, P.V., 1983: The mesoscale and microscale structure and organisation of clouds and precipitation in midlatitude cyclones. VIII: A model for the "seeder–feeder" process in warm frontal rainbands. *J. Atmos. Sci.*, 40, 1185–1206.

Slingo, A. and Schrecker, H.M., 1982: On the short wave radiative properties of stratiform water clouds. *Quart. J. R. Meteor. Soc.*, 108, 407–426.

Smith, R.N.B., 1984: An integrated approach to the representation of cloud processes. E.C.M.W.F., Workshop on Cloud cover parameterization in numerical models, 26–28 November 1984, 233–247 E.C.M.W.F., Shinfield Park, Reading, U.K.

Smith, R.N.B., 1990: A scheme for predicting layer clouds and their water content in a general circulation model. *Quart. J. R. Meteor. Soc.*, 116, 435–460.

Sommeria, G. and Deardorff, J.W., 1977: Subgrid-scale condensation in models of non-precipitation clouds. *J. Atmos. Sci.*, 34, 344–355.

Sun, W.Y. and Ogura, Y., 1980: Modelling the evolution of the convective p.b.d. *J. Atmos. Sci.*, 27, 1558.

Sundqvist, H., 1978: A parametrisation scheme for non-convective condensation including prediction of cloud water content. *Quart. J. R. Meteor. Soc.*, 104, 677–690.

Tapp, M.C. and White, P.W., 1976: A non-hydrostatic mesoscale model, *Quart. J. R. Meteor. Soc.*, 102, 277–296.

Therry, G. and Lacarrère, P., 1983: Improving the eddy kinetic energy model for p.b.d. description. *Boundary Layer Met*, 25, 63.

Tremant, M., 1989: The forecasting of sea fog. *Meteor. Mag.*, 118, 69–75.

Wright, B.J. and Golding, B.W., 1990: The impact of radar and satellite imagery in a mesoscale NWP system. *Weather Radar Networking*, ed Collier, C.G. and Chapius, M., Dordrecht, Kluwer Academic Publishers, 378-390.

Yamada, T. and Mellor, G.L., 1979: A numerical simulation of BOMEX data using a turbulence closure model coupled with ensemble cloud relations, *Quart. J. R. Meteor. Soc.*, 105, 915.

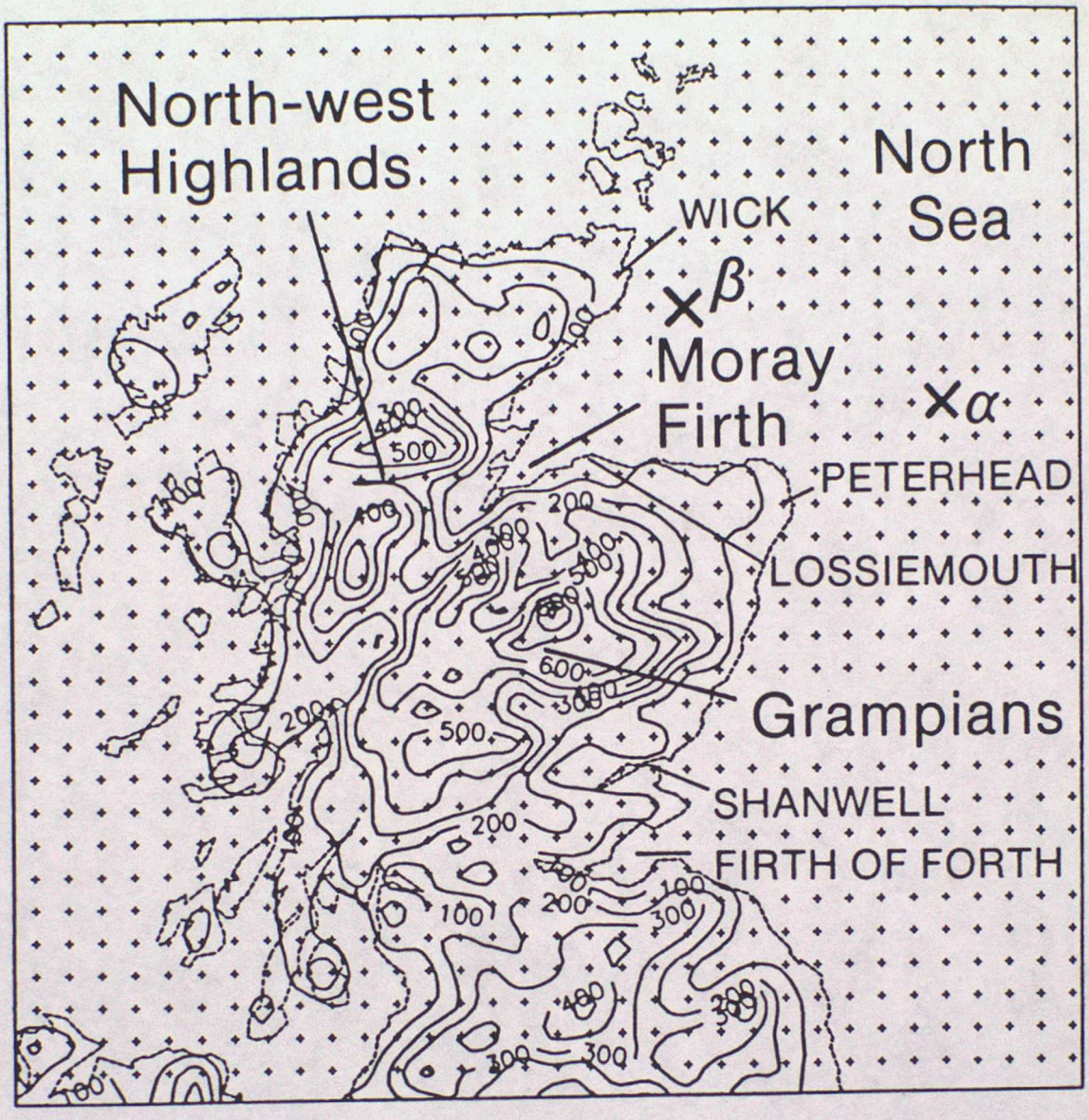

Figure 1. Mesoscale model orography with 100m contours in the area of interest for these simulations. The field study took place in the Moray Firth extending out into the North Sea beyond α and β. + model grid points.

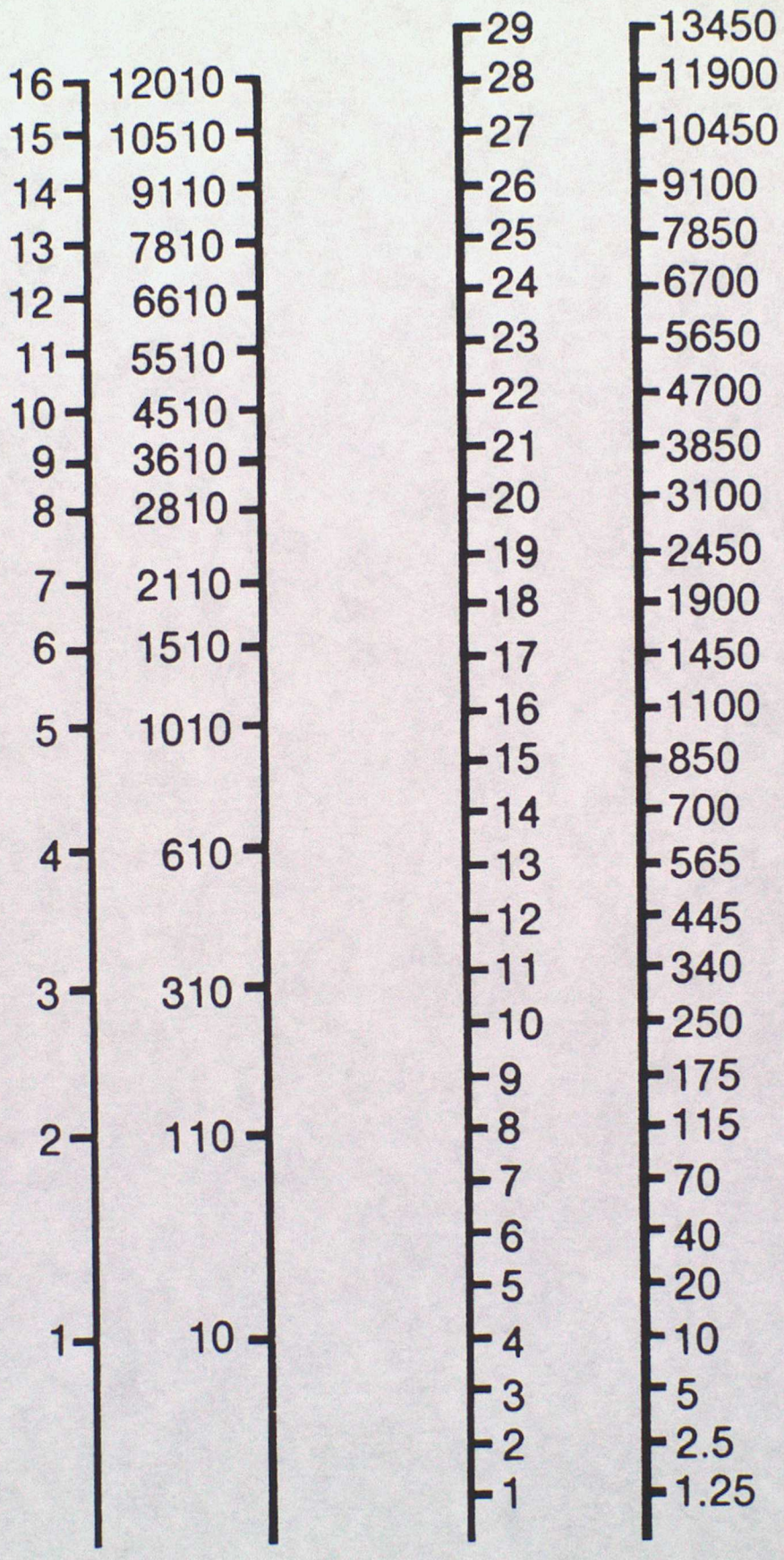

Figure 2. Heights (in metres) of mesoscale model levels.

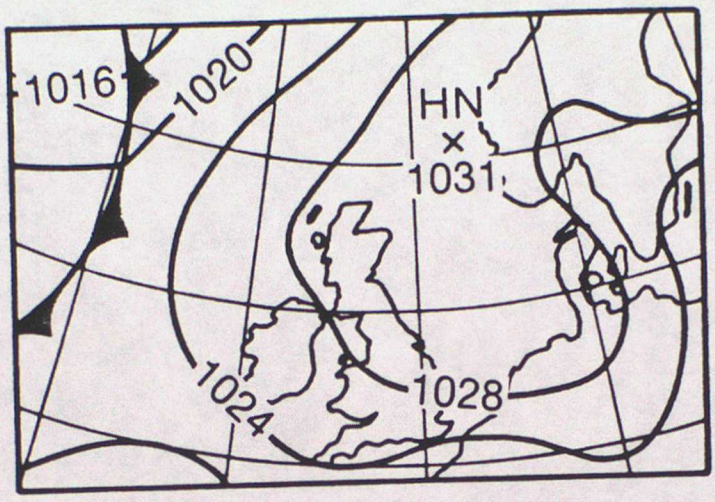

Figure 3. Synoptic situation at 1200 UTC 27 April 1984.

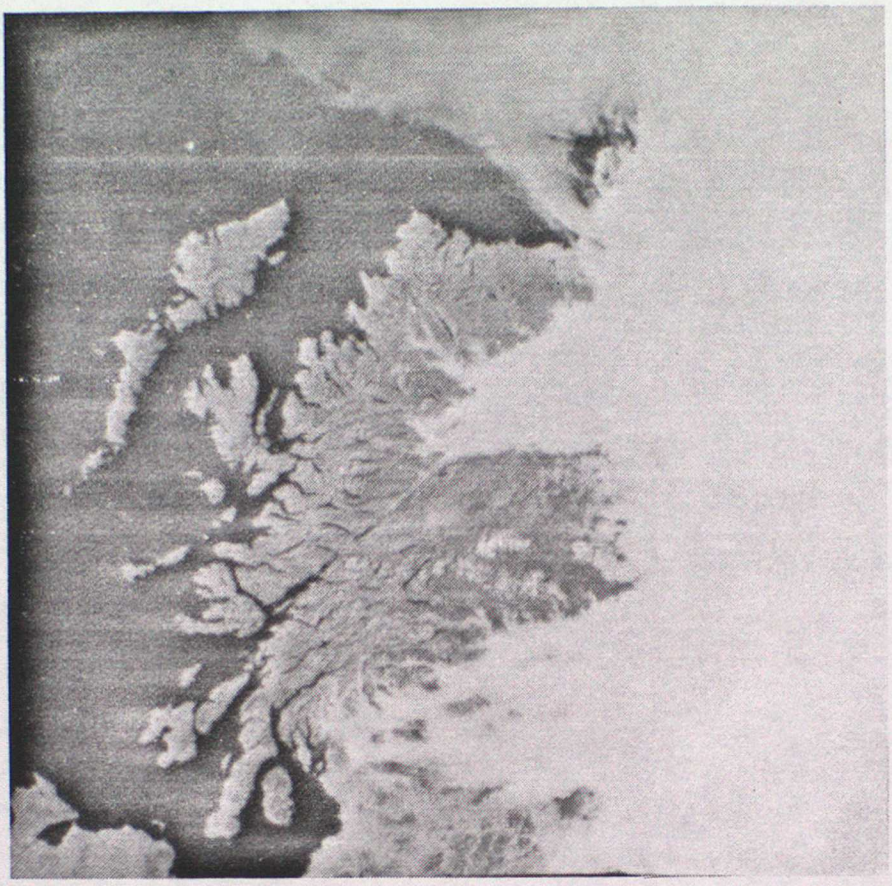

Figure 4a. NOAA-8 visual image at 0836 UTC 27 April 1984

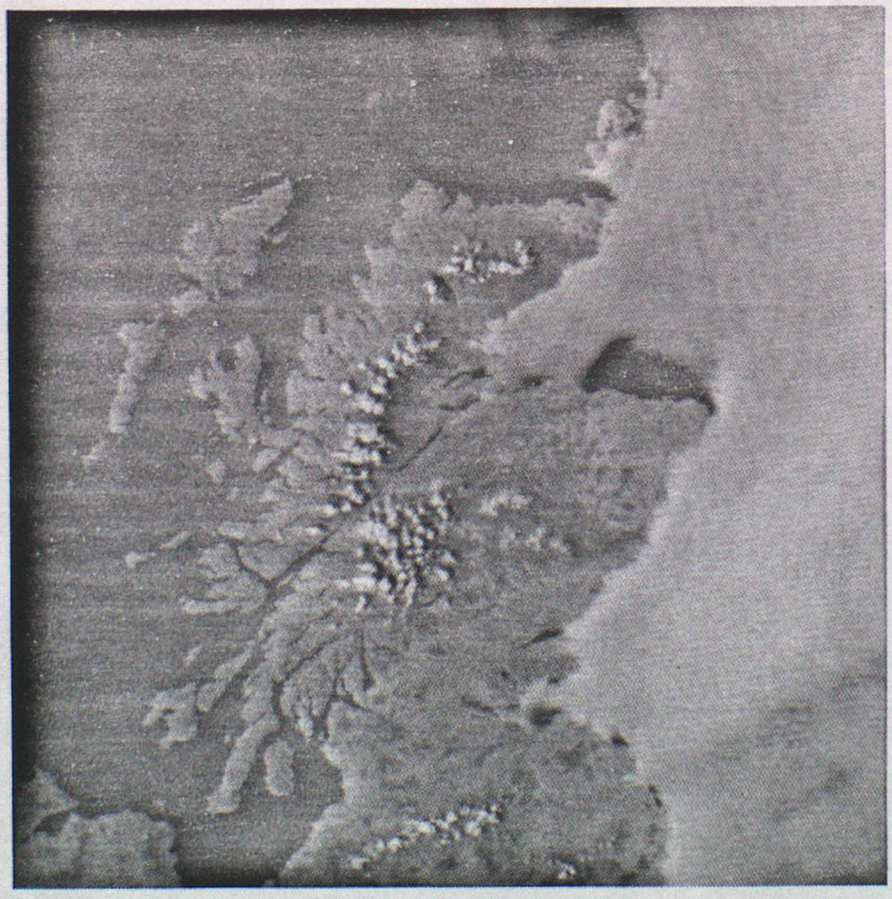

Figure 4b. NOAA-7 visual image at 1448 UTC 27 April 1984

(photographs courtesy of the Electronic Laboratory, University of Dundee)

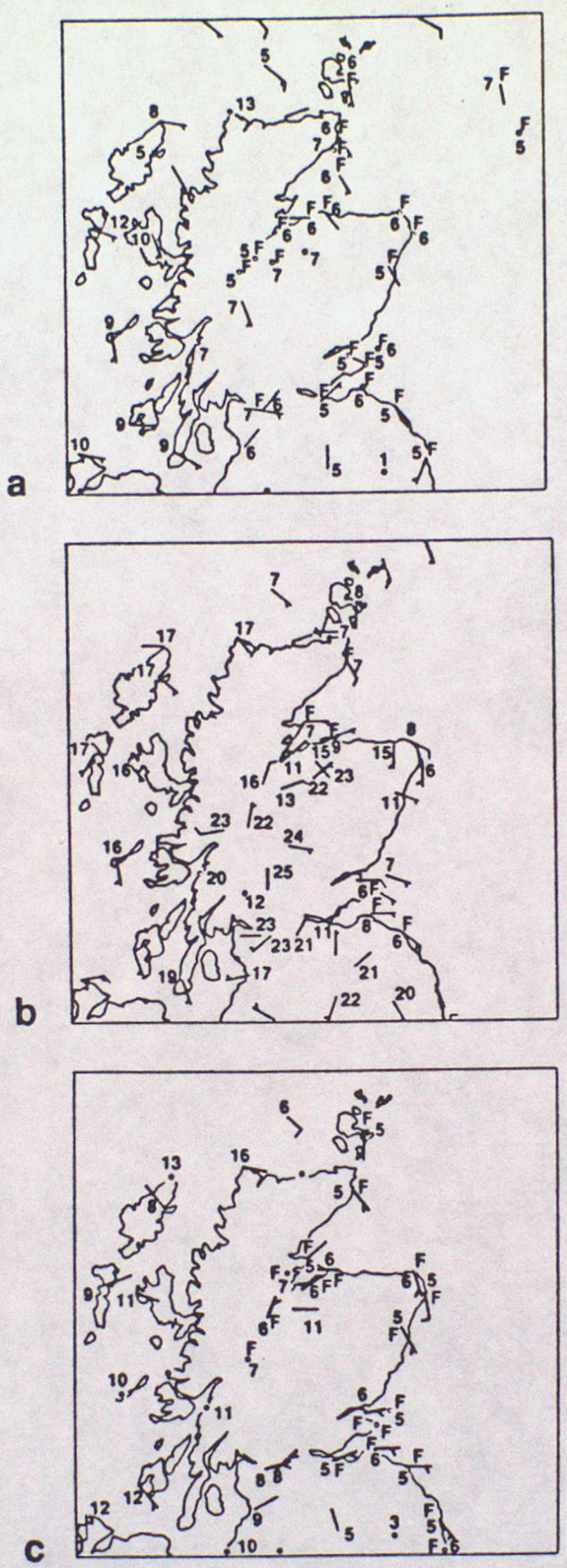

Figure 5. Surface observations of temperature (°C), wind (knots) and fog (F=visibility less than 1 km)

a) 0600 UTC 27 April 1984

b) 1500 UTC 27 April 1984

c) 0000 UTC 28 April 1984

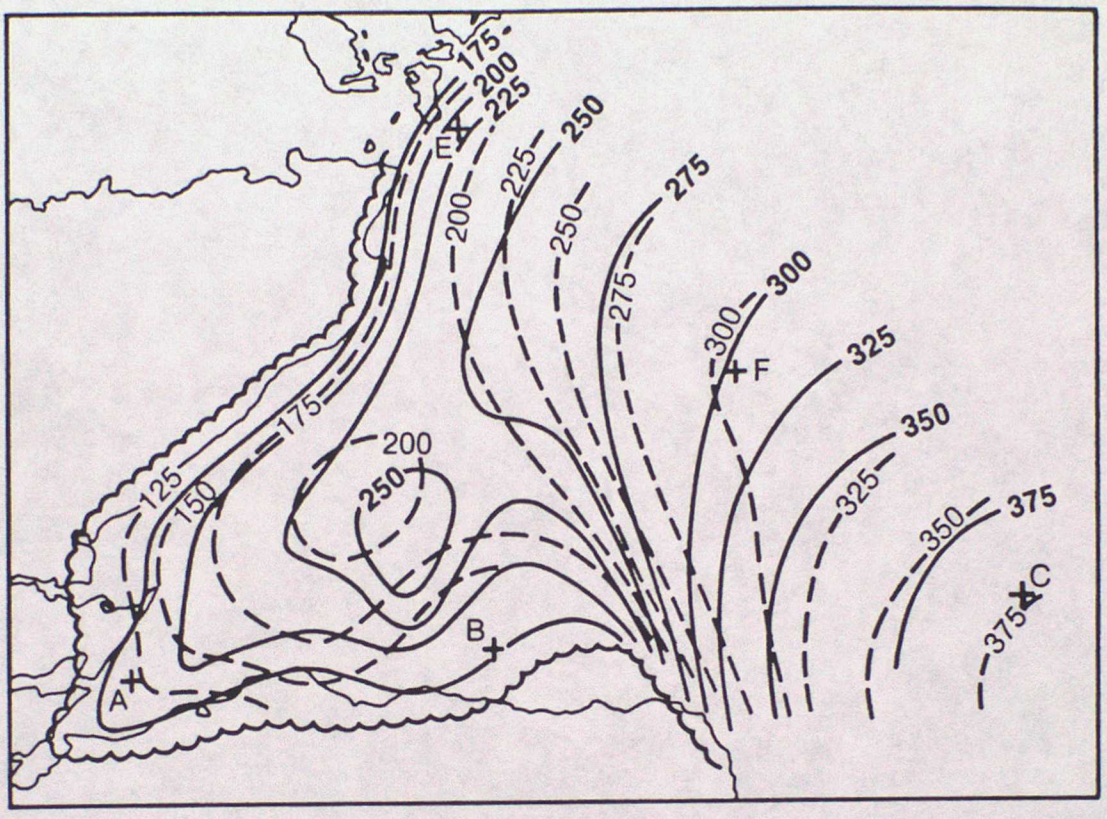

Figure 6. Height of fog top in metres from aircraft flight track A-B-C-F-E-B.

—— 1100–1230 UTC - - - 1230–1400 UTC

ωω estimated fog edge at 1200 UTC.

(figure courtesy of FRH, Quart. J. R. Meteor. Soc.,)

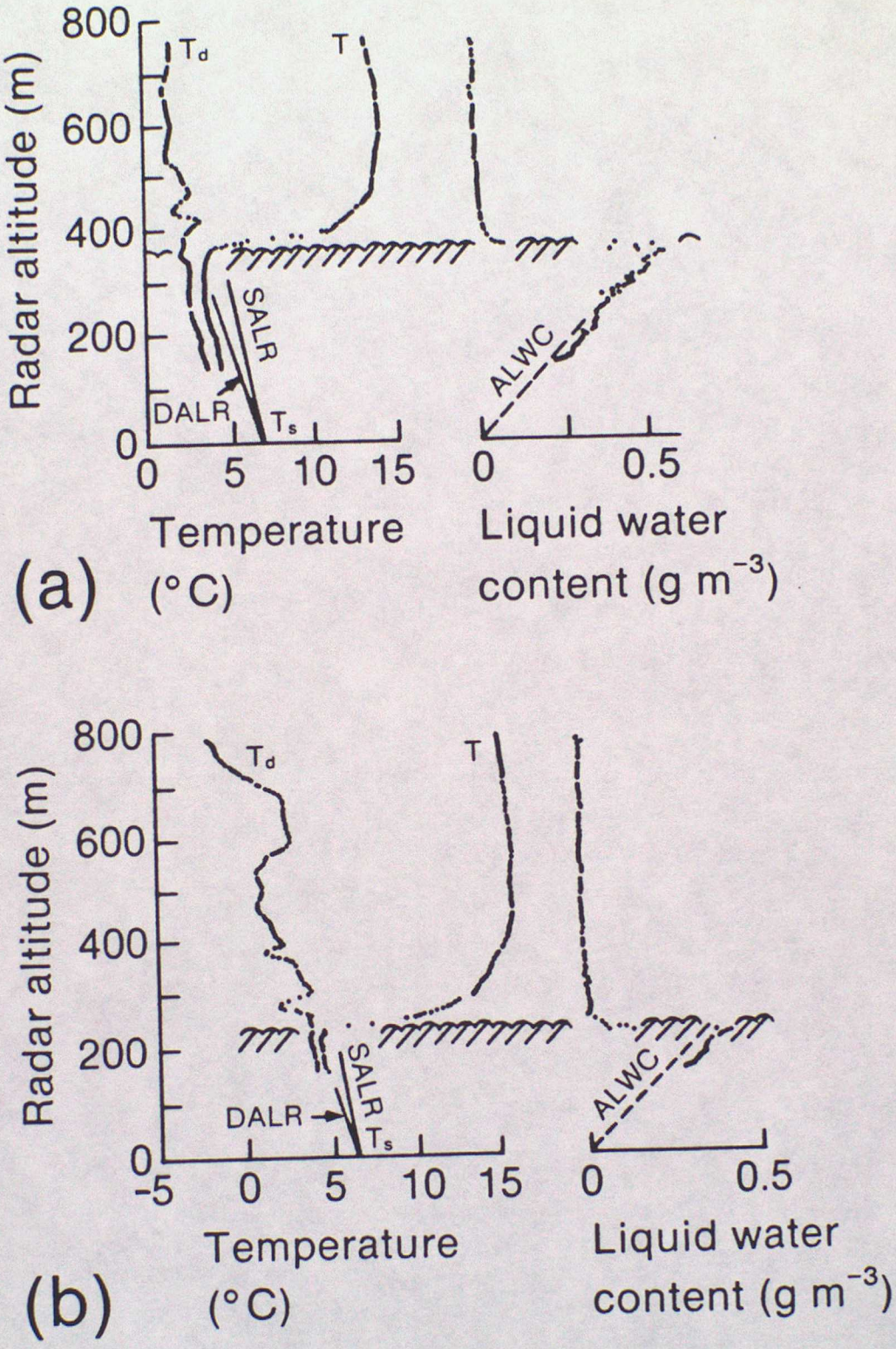

Figure 7. Profiles of temperature, dew point and cloud water from aircraft data.

a) Deep fog at α at 1154 UTC

b) Shallower fog at β at 1230 UTC

positions of α and β are shown in figure 1.

(figure courtesy of FRH, Quart. J. R. Meteor. Soc.,)

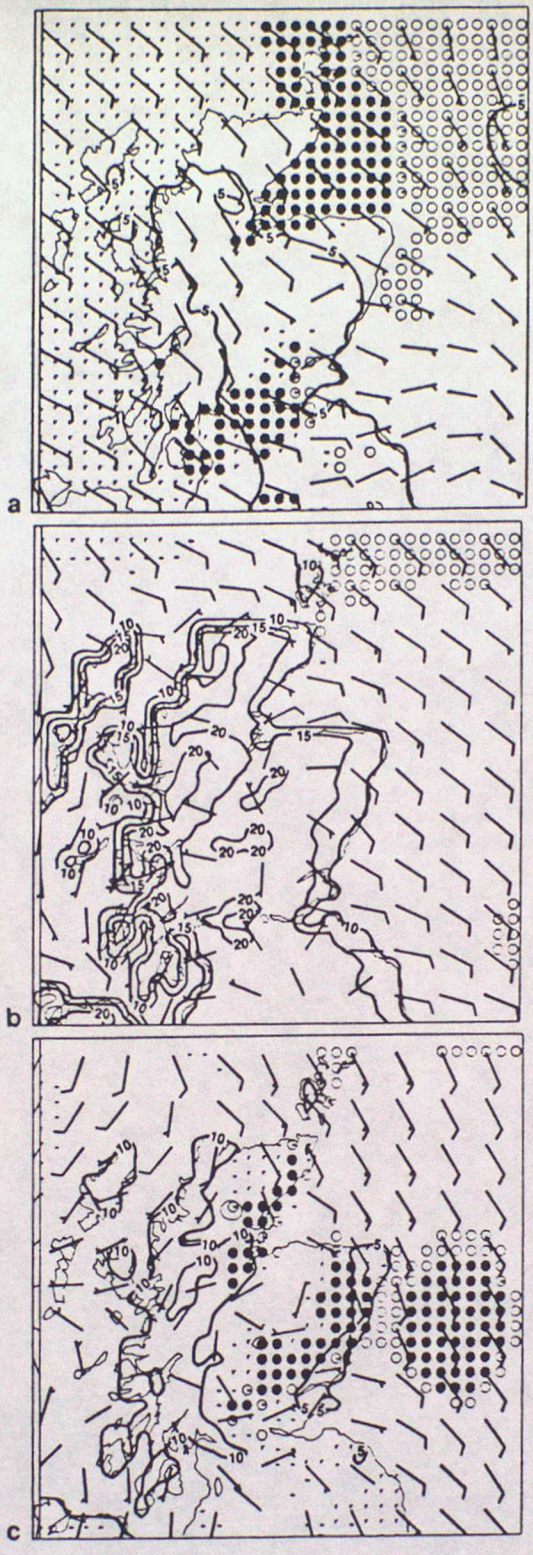

Figure 8. Mesoscale model initial conditions and forecast fields for the 16 level version run from interpolated regional model fields.

a) initial conditions at 0600 UTC 27 April 1984

b) T+9 forecast fields for 1500 UTC 27 April 1984

c) T+18 forecast fields for 0000 UTC 28 April 1984

F = Surface fog with top at 10m

• = Surface fog with top at least 110m

o = low cloud/fog with base above 10m

- = mist (visibility at 10m 1–5km)

Also shown are surface temperature at 5°C contour intervals and surface wind (at 10m) in knots.

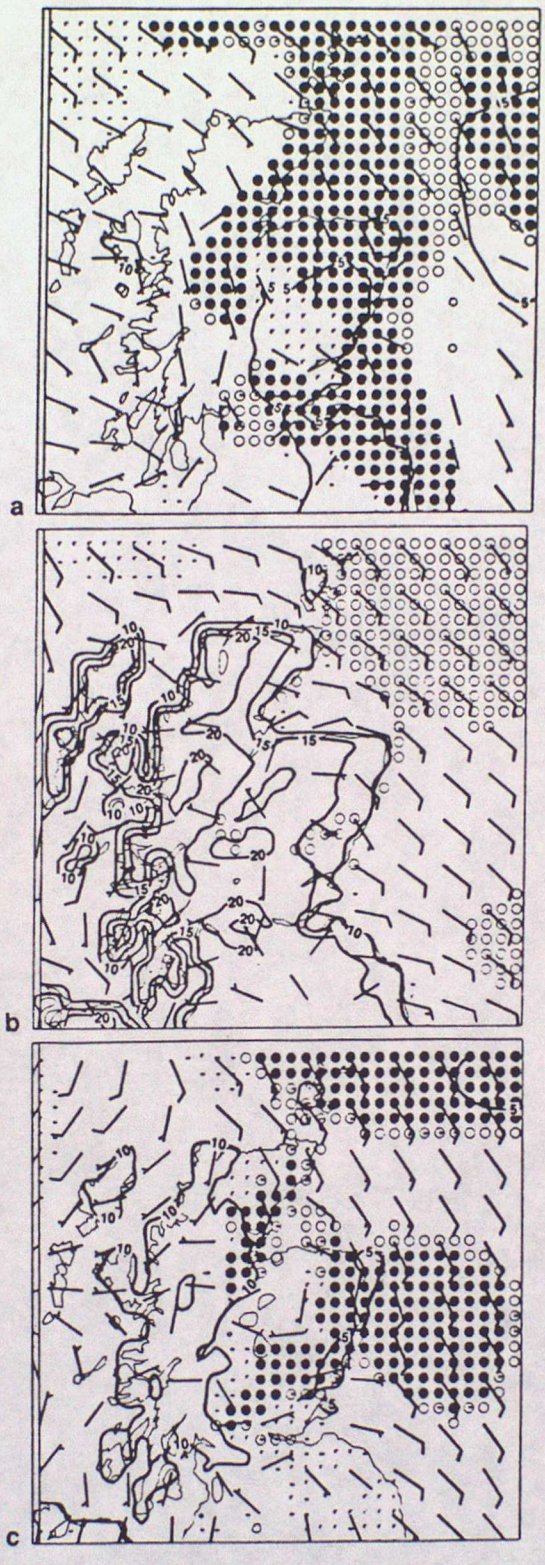

Figure 9. Mesoscale model initial conditions and forecast fields for the 16 level version run from interpolated regional model fields modified by surface observations.

a) initial conditions at 0600 UTC 27 April 1984

b) T+9 forecast fields for 1500 UTC 27 April 1984

c) T+18 forecast fields for 0000 UTC 27 April 1984

Symbols as figure 8.

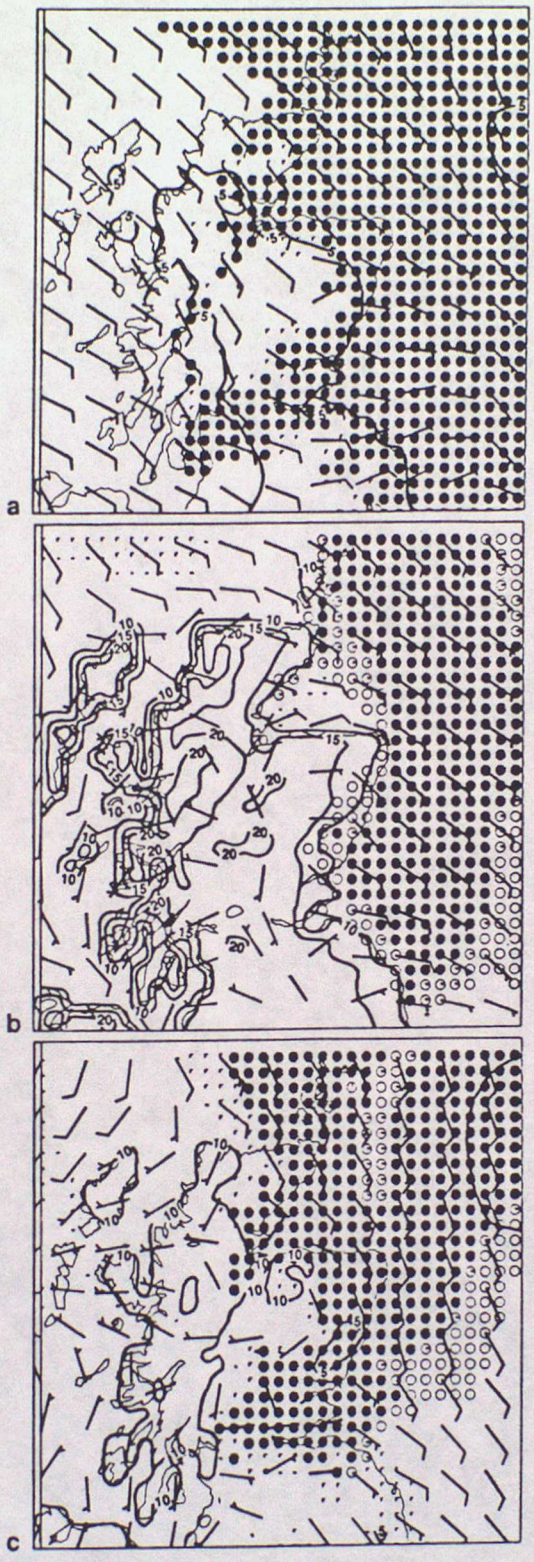

Figure 10. Mesoscale model initial conditions and forecast fields for the 16 level version run from interpolated regional model fields.

a) initial conditions at 0600 UTC 27 April 1984

b) T+9 forecast fields for 1500 UTC 27 April 1984

c) T+18 forecast fields for 0000 UTC 28 April 1984

Symbols as figure 8.

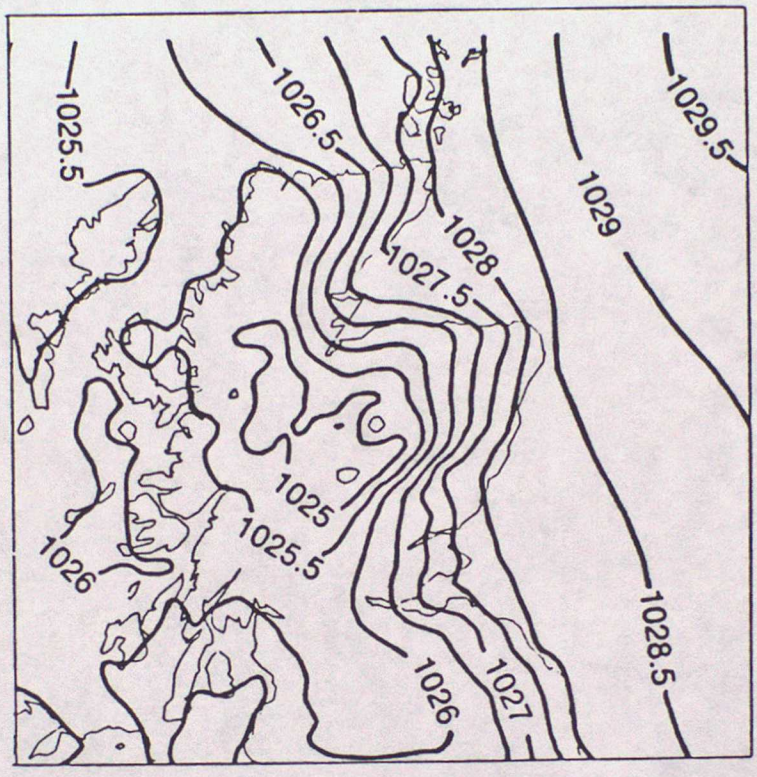

Figure 11. Forecast mean sea level pressure at 1500 UTC 27 April 1984 from the 16 level forecast run from interpolated regional model fields modified by use of satellite imagery and profile data.

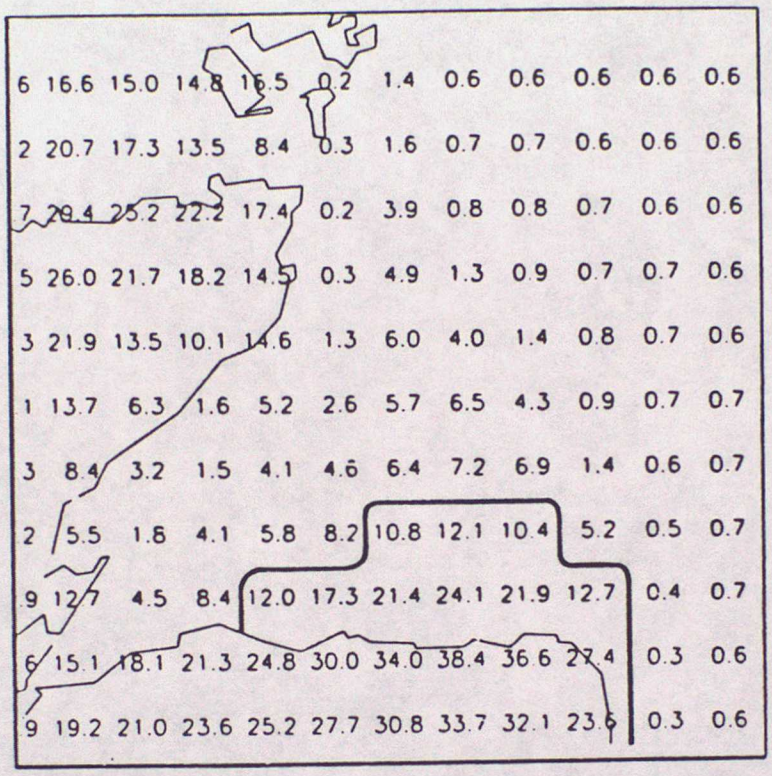

Figure 12. Forecast visibility at 10m in the Moray Firth area for 1500 UTC 27 April 1984 from the 16 level forecast run from interpolated regional model fields modified by use of satellite imagery and profile data. The boundary of the area of visibilities greater than 10 km in the south of the Moray Firth is marked.

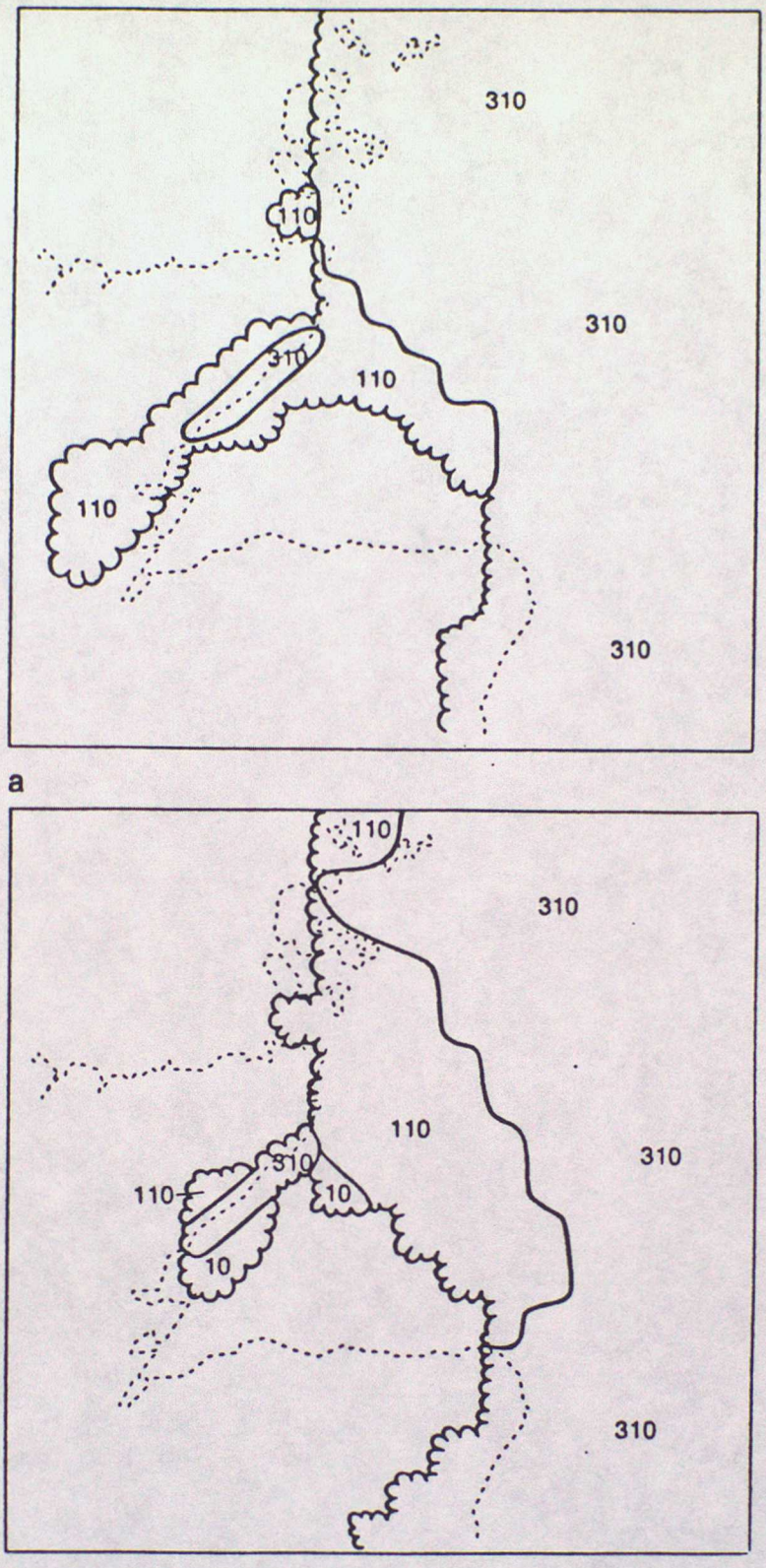

Figure 13. Forecast fog top heights in metres in the Moray Firth area during the afternoon of 27 April 1984 from the 16 level forecast run from interpolated regional model fields modified by use of satellite imagery and profile data. ⌇⌇⌇ forecast fog edge

a) at 1200 UTC

b) at 1500 UTC

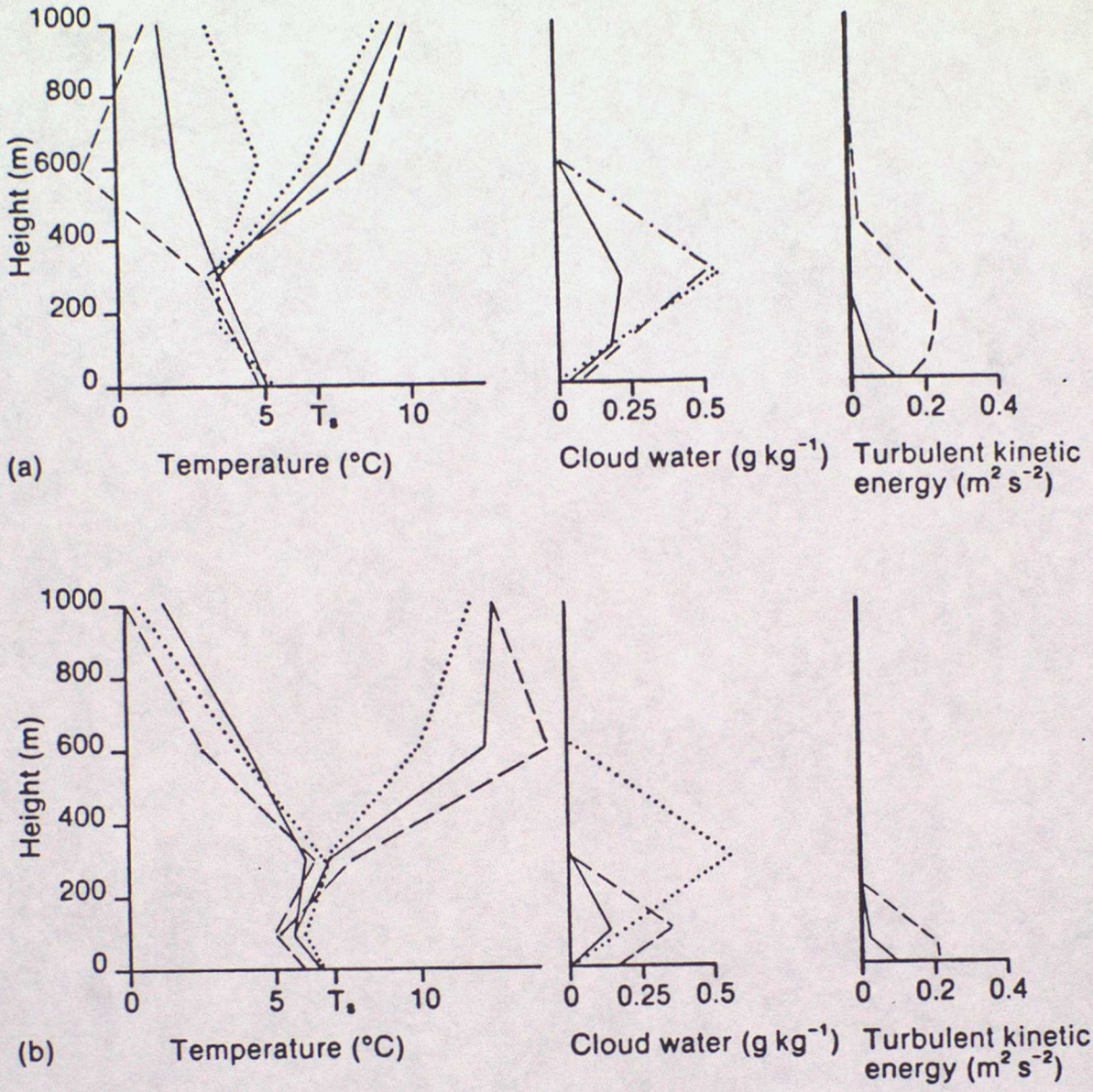

Figure 14. Initial and forecast profiles of temperature, dew point and cloud water and forecast profiles of turbulent kinetic energy from the 16 level forecast run from interpolated regional model fields modified by use of satellite imagery and profile data.

a) profiles at α , b) profiles at β

positions of α and β are shown in figure 1.

. . . . . initial profiles ____ profiles at 1200 UTC 27 April 1984

_ _ _ profiles at 0000 UTC 28 April 1984

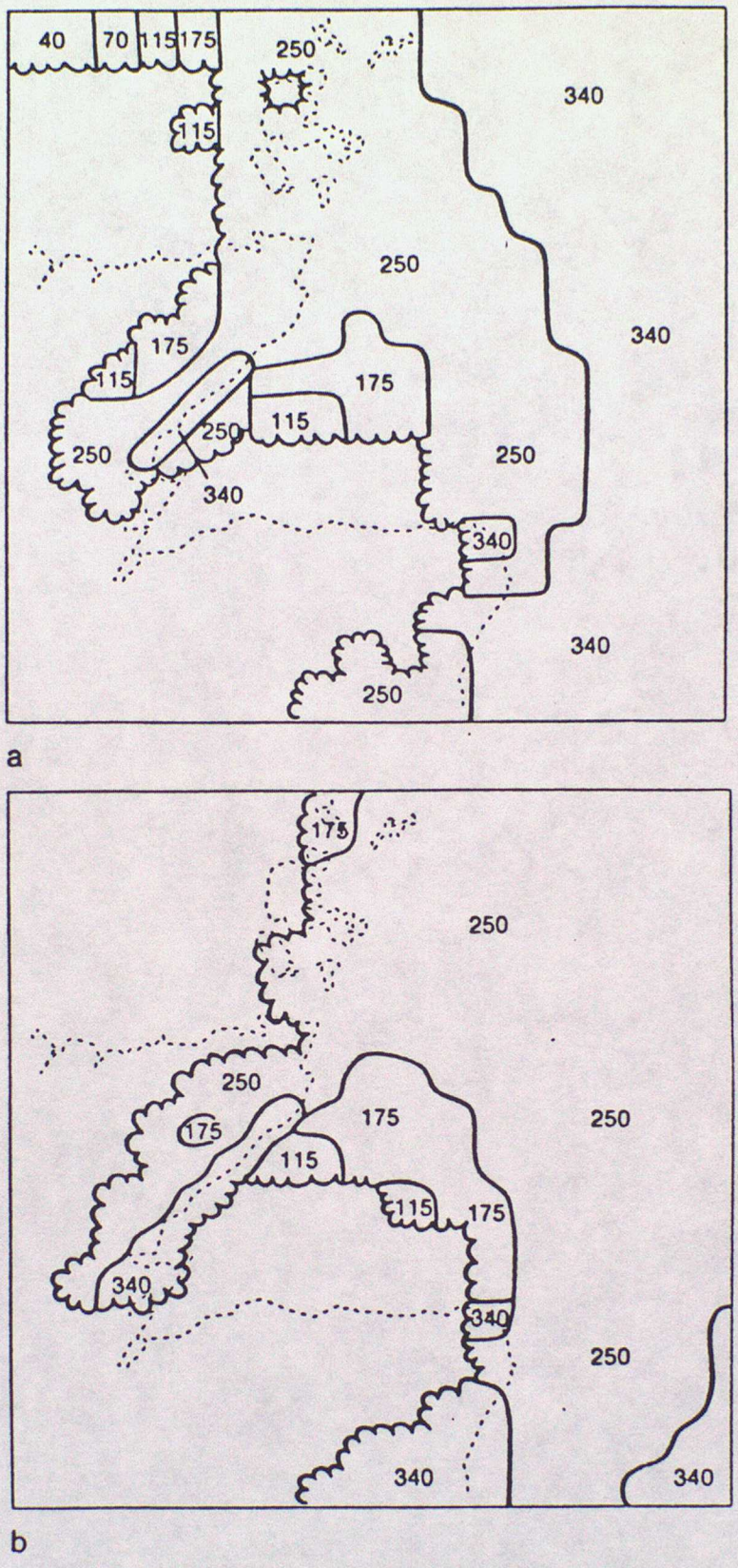

Figure 15. Forecast fog top heights in metres in the Moray Firth area during the afternoon of 27 April 1984 from the 29 level forecast run from interpolated regional model fields modified by use of satellite imagery and profile data. ∪∪∪ forecast fog edge

a) at 1200 UTC

b) at 1500 UTC

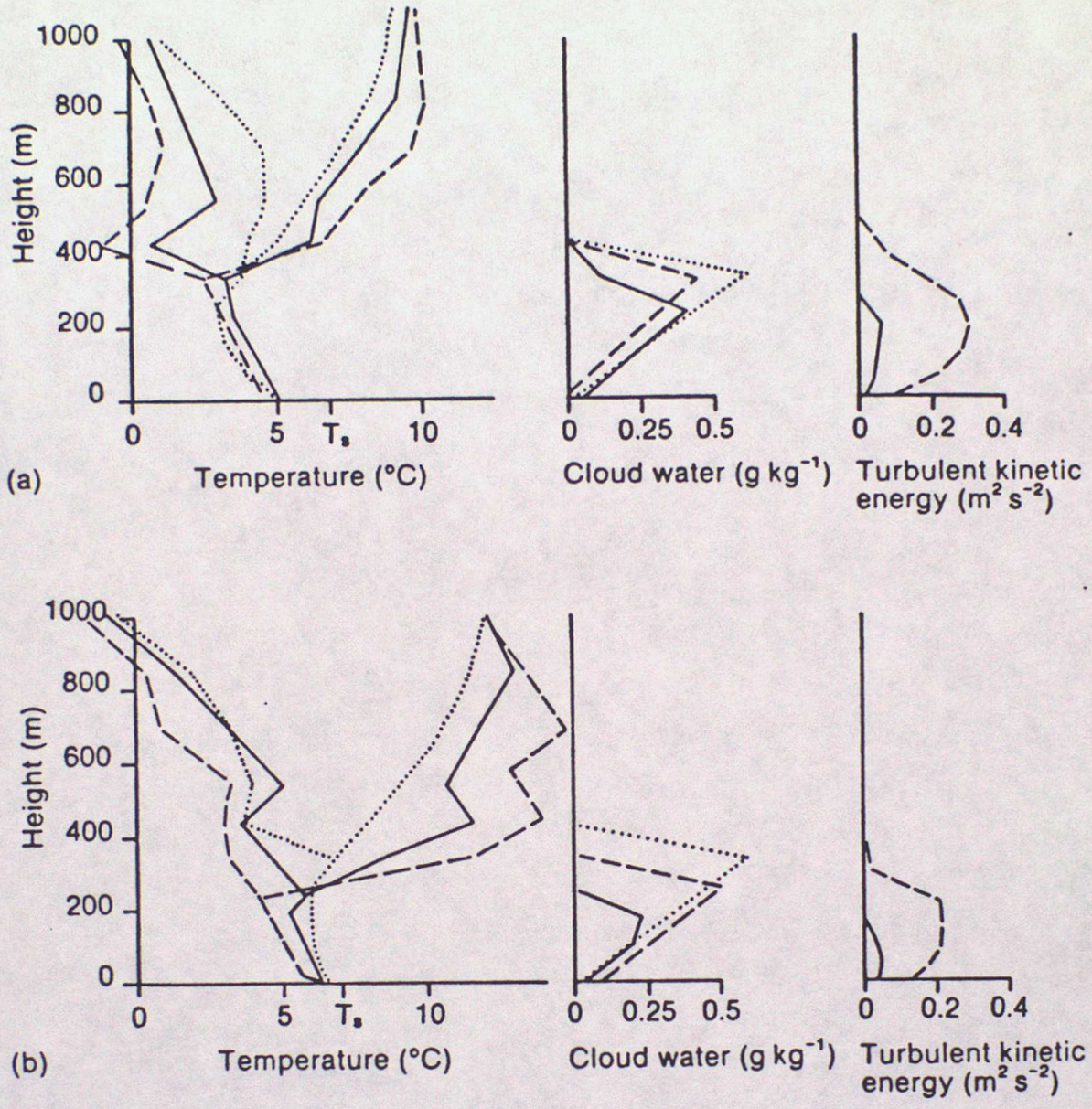

Figure 16. Initial and forecast profiles of temperature, dew point and cloud water and forecast profiles of turbulent kinetic energy from the 29 level forecast run from interpolated regional model fields modified by use of satellite imagery and profile data.

a) profiles at α , b) profiles at β

positions of α and β are shown in figure 1.

. - - - initial profiles ____ profiles at 1200 UTC 27 April 1984

_ _ _ profiles at 0000 UTC 28 April 1984

CURRENT SHORT - RANGE FORECASTING RESEARCH SCIENTIFIC NOTES (OCTOBER 1990)

The Short- Range Forecasting Research Branch (formerly Met O 11) Scientific Notes which contain information of current use are listed below. The complete set of Scientific Notes is available from the National Meteorological Library on loan, if required.

1. The theory of periodic solutions of the semi-geostrophic equations.
R.J. Purser
October 1987

2. Properties of the partial differential equations governing various types of atmospheric motions and implications for numerical methods.
M.J.P. Cullen
December 1987

3. A geometric model of balanced, axisymmetric flows with embedded penetrative convection.
G.J. Shutts, M. Booth and J. Norbury
February 1988

4. Implicit finite difference methods for computing discontinuous atmospheric flows.
M.J.P. Cullen
March 1988

5. Variational aspects of semi-geostrophic theory.
R.J. Purser
August 1988

6. On the incorporation of atmospheric boundary layer effects into a balanced model.
M.J.P. Cullen
July 1988

7 Implicit finite difference methods for modelling discontinuous atmospheric flows.
M.J.P. Cullen
June 1988

8. An analytical model of the growth of a frontal intrusion.
M.W. Holt and G.J. Shutts
November 1988

9. Planetary semi-geostrophic equations derived from Hamilton's principle.
G.J. Shutts
July 1988

10. Semi-geostrophic moist frontogenesis in a Lagrangian model.
M.W. Holt
September 1988

11. Generalised Lagrangian solutions for atmospheric and ocean flows.
M.J.P. Cullen, J. Norbury and R.J. Purser
November 1988

CURRENT SHORT - RANGE FORECASTING RESEARCH SCIENTIFIC NOTES (OCTOBER 1990) CONTINUED

12. Properties of the Lagrangian semi-geostrophic equations.
M.J.P. Cullen and R.J. Purser
January 1989

13. A simple two phase precipitation scheme for use in numerical weather prediction models.
B.W. Golding
June 1989

14. A test of a semi-implicit integration technique for a fully compressible non-hydrostatic model.
M.J.P. Cullen
September 1989

15. Dynamical aspects of the October storm 1987 : A study of a successful Fine-mesh simulation
G.J. Shutts
September 1989

16. A conservative split-explicit integration scheme suitable for forecast and climate models.
M.J.P. Cullen and T. Davis
January 1990

17. The dynamical structure of some North Atlantic depressions simulated by the fine-mesh model.
G.J.Shutts
January 1990

18. An Idealised Simulation of the Indian Monsoon using Primitive Equation and Quasi - Equilibrium models.
M.H. Mawson and M.J.P. Cullen
August 1990

19. Time - Integration Schemes for meteorological simulations involving oscillatory and dissipative modes.
R.J. Purser
July 1990

20. Mesoscale Model Experimental forecasts of the Haar of North East Scotland.
S.P. Ballard, B.W.Golding, R.N.B. Smith
August 1990